Pergamon

0148-9062(95)00036-4

Int. J. Rock Mech. Min. Sci. & Geomech. Abstr. Vol. 32, No. 5, pp. 465–479, 1995

0148-9062/95 $9.50 + 0.00

Coupled Thermal-Mechanical-Hydrological Behaviour of Sparsely Fractured Rock: Implications for Nuclear Fuel Waste Disposal

T. S. NGUYEN†
A. P. S. SELVADURAI‡

This paper summarizes research activities on thermal-mechanical-hydrological (TMH) coupling and its implications on nuclear fuel waste disposal in sparsely fractured plutonic rocks. These research activities include the development of a finite element computer code, FRACON, its verification against analytical solutions, its calibration against laboratory and field experiments initiated by the Atomic Energy Control Board (AECB) and performed at Carleton and McGill Universities, and the AECB's participation in the DECOVALEX international project. The FRACON code was used in the preliminary analysis of the coupled TMH response of a sparsely fractured rock mass around a hypothetical nuclear fuel waste repository. It was found that the flow and structural characteristics of this rock mass could be significantly perturbed by the thermal pulse generated by the wastes. The implications of these perturbations on the safety of the disposal system have to be further quantified.

1. INTRODUCTION

In Canada, nuclear fuel waste (NFW) disposal in sparsely fractured plutonic rocks is being currently proposed by Atomic Energy of Canada Ltd (AECL) [1]. The geological barrier is a major one in that proposal [2]. The performance of the geological barrier ultimately depends on its groundwater regime. Since the wastes will generate heat for hundreds to thousands of years, the stability, deformation and water flow characteristics of the rock mass will be influenced by the introduced thermal pulse. To develop plausible models of coupled thermal-hydrological-mechanical (THM) processes in geological media, it is desirable to consider the characteristics of both the intact rock and discontinuities such as fracture zones that are usually present in massive geological formations. An extensive literature review has shown that the study of coupled THM processes in porous, sparsely fractured geological media, such as granitic rock of the Canadian Shield are still in a relatively early stage of theoretical and experimental development. Specific questions of interest could include the following aspects:

(i) The progress in code development of THM coupled processes has been hindered by the scarcity of both available analytical solutions to perform verification, and experimental data to perform calibration/validation. This fact has been widely recognized by many researchers [3–8].
(ii) Conversely, the design of laboratory of *in situ* experiments and the interpretation of the results are problematic without adequate mathematical models capable of simulating the experiments. Thus, computational modelling and experimental modelling should be regarded as complementary endeavours.
(iii) Although Terzaghi's and Biot's [9, 10] theories of isothermal consolidation have been successfully used to predict certain aspects of the consolidation behaviour of soils, more studies are needed in order to extend these theories to sparsely jointed rocks, especially in the non-isothermal range.
(iv) In order to handle complex geometries and boundary conditions, numerical methods, such as the finite element, boundary integral element or discrete element methods, need to be developed. The finite element method is the computational modelling procedure that is most widely used by engineers. With finite element modelling of non-isothermal consolidation problems, numerical difficulties, in the form of spatial and temporal oscillations of the solutions, could be experienced.

The Atomic Energy Control Board (AECB) is the Canadian agency responsible for the regulation of the

†Atomic Energy Control Board, Wastes and Impacts Division, 280 Slater, Ottawa, Ontario, Canada K1P 59.
‡McGill University, Montreal, Canada H3A 2K6.

nuclear industry in Canada. In order to independently assess the implications of THM coupling on NFW disposal in sparsely fractured plutonic rocks, as being currently proposed by AECL, the AECB has initiated a research program, in cooperation with Carleton University and McGill University which consists of two main phases:

(i) Develop a finite element code, FRACON, with a variety of element capabilities which can examine THM processes in both solid media and in discontinuities. Verify the code against analytical solutions and calibrate/validate the code against laboratory and field experiments.
(ii) Simulate the coupled THM behaviour of a hypothetical NFW repository. Perform parametric studies to examine the influences of jointing, stress-dependence of permeability, nonlinear stress–strain behaviour (particularly for fractures and joints), etc. on the performance of the hypothetical NFW repository.

In this paper, we will present the progress achieved to date in the above research programme.

2. GOVERNING EQUATIONS OF COUPLED THM PROCESSES IN SATURATED GEOLOGICAL MEDIA—FINITE ELEMENT FORMULATION

By generalizing Biot's theory of consolidation to include thermal effects, we can obtain the following equations governing the non-isothermal consolidation of saturated porous media [11]:

$$\frac{\partial}{\partial x_i}\left(\kappa_{ij}\frac{\partial T}{\partial x_j}\right)=\rho C\frac{\partial T}{\partial t} \tag{1}$$

$$G\frac{\partial^2 u_i}{\partial x_j \partial x_j}+(G+\lambda)\frac{\partial^2 u_j}{\partial x_i \partial x_j}+\alpha\frac{\partial p}{\partial x_i}-\beta K_D\frac{\partial T}{\partial x_i}+F_i=0 \tag{2}$$

$$\frac{\partial}{\partial x_i}\left[\frac{k_{ij}}{\mu}\left(\frac{\partial p}{\partial x_j}+\rho_f g_j\right)\right]-\left(\frac{n}{K_f}-\frac{n}{K_s}+\frac{\alpha}{K_s}\right)\frac{\partial p}{\partial t}+\alpha\frac{\partial}{\partial t}\left(\frac{\partial u_i}{\partial x_i}\right)+[(1-\alpha)\beta-(1-n)\beta_s-n\beta_f]\frac{\partial T}{\partial t}=0 \tag{3}$$

where the unknowns are the displacement u_i (m), temperature T (°C) and pore pressure p (Pa), κ_{ij} is the thermal conductivity tensor of the bulk medium (W/m/°C), ρ is the density of the bulk medium (kg/m^3), C is the specific heat per unit mass of the bulk medium (J/kg/°C), G and λ are the Lame's constants (Pa), $\alpha=1-K_D/K_s$, K_D, K_s and K_f are, respectively, the bulk modulii of the drained material, the solid phase and the fluid phase (Pa), F_i is the volumetric body force (N/m^3), β, β_s and β_f are, respectively, the coefficient of thermal expansion of the drained material, the solid phase and the fluid phase (°C^{-1}), n is the porosity of the medium (dimensionless), ρ_f is the density of the fluid (kg/m^3), μ is the viscosity of the fluid (kg/m/sec), k_{ij} is the intrinsic permeability tensor (m^2) and g_i is the ith component corresponding to the acceleration due to gravity (m/sec^2).

In the above equations, the Cartesian tensor notation, with Einstein's summation convention on repeated indices is adopted. In addition, the sign convention for stress and fluid pressure is considered positive for tension fields. In developing these equations, we invoke the basic principles of continuum mechanics (namely conservation of mass, momentum and energy). These principles are universally applicable, independent of the nature of the medium being considered. Also, in order to arrive at a set of equations in which the number of unknowns equals the number of equations, the following additional assumptions are necessary:

(i) Darcy's law governing pore fluid flow. Darcy's law is applicable with reasonable accuracy to almost all types of geological materials [12] including soils and rocks, provided that the hydraulic gradients are within the laminar flow range, and above a threshold gradient within which the pore fluid is virtually immobile.

For most geotechnical applications, the pore fluid is water at a constant temperature, and the original form of Darcy's law is appropriate. Where thermal effects are important, and/or the pore fluid is not water, Darcy's law has to be modified [13], i.e.:

$$V_{if}-V_{is}=\frac{k_{ij}}{n\mu}\left(\frac{\partial p}{\partial x_j}+\rho_f g_j\right). \tag{4}$$

V_{if}, V_{is} are the velocities, respectively, of the fluid and the solid (m/s).

The use of the generalized Darcy's law (4) is essential when one deals with fluids other than water. It is thus necessary to separate the expression for the hydraulic conductivity K_{ij} (loosely referred to as the permeability in most geotechnical applications) into a fluid independent component k_{ij}, and a fluid dependent component characterized by its viscosity and density, i.e.:

$$K_{ij}=\frac{\rho_f g}{\mu}k_{ij}. \tag{5}$$

The viscosity and density of a particular fluid are also strongly temperature-dependent. When thermal effects are considered, appropriate experimentally derived functions of temperature should be used for these two properties.

(ii) A generalized principle of effective stress is adopted. Several forms of this principle exist [14, 15]. We adopt the form of generalized principle of effective stress formulated by Zienkiewicz *et al.* [15]. In contrast to Terzaghi's principle of effective stress [9], this generalized principle takes into consideration the compressibility of the pore fluid and the solid phases. Omission of the compressibility of the pore fluid and the solid phase could lead to an overprediction of pore pressures in competent rocks [11].

(iii) Hooke's law for linear isotropic elastic behaviour of the porous skeleton is adopted. This is a useful first approximation for the study of intact competent rocks which are subjected to stress states below those which could initiate fracture, failure or damage. More sophisticated constitutive relationships could be introduced and these will be considered in the future developments of this work.

(iv) Heat conduction is assumed to be the predominant mechanism of heat transfer. In a geological medium, there are two dominant mechanisms of heat transfer—heat conduction and heat convection. Heat conduction is the transfer of heat by the activation of solid and fluid particles, without their bulk movement. The conduction of heat is governed by Fourier's law, which states that the rate of heat flow is proportional to the temperature gradient. Heat convection on the other hand is due to the bulk motion of the particles. In a poro-elastic medium, the movement or displacement of the solid particles could be neglected; thus it is the fluid flow which is primarily responsible for the convective heat transfer. The rate of heat transfer by convection is proportional to the rate of fluid flow. It could be shown that for low permeability geological media, such as granitic rock masses, since the rate of fluid flow is sufficiently slow, heat transfer by convection is usually negligible in comparison to heat transfer by conduction.

We assume that conduction is the main mechanism of heat transfer, and that Fourier's law applies. We also assume that a state of thermal equilibrium always exists between the fluid and the solid (i.e. at any point, the temperature of the solid equals the temperature of the fluid).

The governing equations are approximated by matrix equations via a standard Galerkin finite element procedure [13]. Let us consider a domain R with boundary B where the above equations apply. Considering standard finite element procedures, the domain R is discretized in N_e elements. Two types of elements are considered:

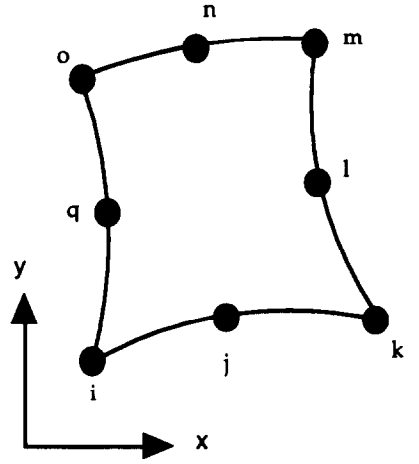

Fig. 1. Solid isoparametric element.

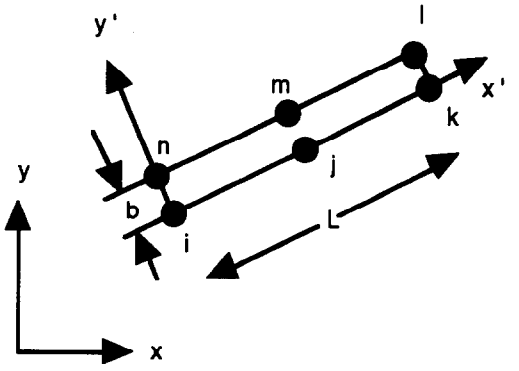

Fig. 2. Joint element.

Plane isoparametric elements. This element (Fig. 1) is used to represent the unfractured rock mass. Displacements within the element are interpolated as functions of the displacements at all eight nodes, while the pore pressure and temperature are interpolated as functions of the same values at only the four corner nodes i, k, m and o. A detailed description of this element is given, for example, by Smith and Griffiths [16].

Joint element. This element (Fig. 2) is used to simulate discontinuities in the rock mass such as joints, fracture zones, and fault zones. In finite element terminology [17–21], it is a very thin element, characterized by a thickness b and length L. Nodal displacements are obtained at all six nodes (Fig. 2) while nodal pore pressures and temperatures are obtained only at the corner nodes i, k, l and n. The mechanical behaviour of the element is dictated by its shear and normal stiffnesses $D_{x'y'}$ and $D_{y'y'}$, respectively, and its hydraulic and thermal behaviour are governed by the transverse and longitudinal permeabilities $k_{y'y'}$ and $k_{x'x'}$, and the transverse and longitudinal thermal conductivities $k_{y'y'}$ and $k_{x'x'}$, respectively.

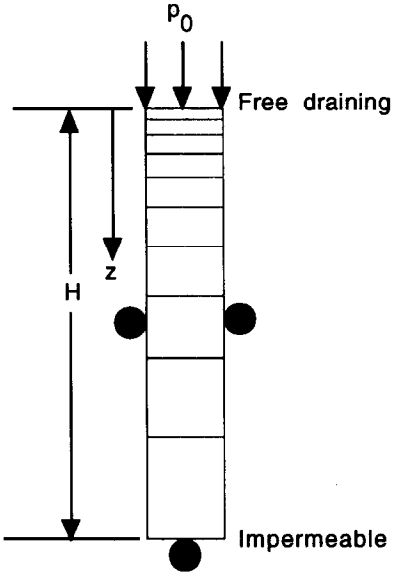

Fig. 3. Finite element mesh for one-dimensional isothermal consolidation.

With the above two types of elements being fully defined, a Galerkin procedure is applied to the differential equations (1)–(3) of non-isothermal consolidation. One then obtains the matrix equations of the form:

$$[\theta[\mathbf{KH}] + (\rho C/\Delta t)[\mathbf{CM}]]\{\mathbf{T}\}^1 = \{\mathbf{FH}\} + \{\mathbf{FQ}\} + [(\theta - 1)[\mathbf{KH}] + (\rho C/\Delta t)[\mathbf{CM}]]\{\mathbf{T}\}^0 \quad (6)$$

$$\begin{bmatrix} [\mathbf{K}] & \alpha[\mathbf{CP}] \\ \alpha[\mathbf{CP}]^T & -\theta\Delta t[\mathbf{KP}] - c_e[\mathbf{CM}] \end{bmatrix} \begin{Bmatrix} \{\mathbf{d}\}^1 \\ \{\mathbf{p}\}^1 \end{Bmatrix} = \{\mathbf{f}\} + \begin{bmatrix} \frac{\theta - 1}{\theta}[\mathbf{K}] & \alpha\frac{\theta - 1}{\theta}[\mathbf{CP}] \\ \alpha[\mathbf{CP}]^T & (1 - \theta)\Delta t[\mathbf{KP}] - c_e[\mathbf{CM}] \end{bmatrix} \begin{Bmatrix} \{\mathbf{d}\}^0 \\ \{\mathbf{p}\}^0 \end{Bmatrix} + \begin{bmatrix} \frac{\beta K_D}{\theta}[\mathbf{K}] & [\mathbf{0}] \\ [\mathbf{0}] & \beta_e[\mathbf{CM}] \end{bmatrix} \begin{Bmatrix} (1 - \theta)\{\mathbf{T}\}^0 + \theta\{\mathbf{T}\}^1 \\ \{\mathbf{T}\}^1 - \{\mathbf{T}\}^0 \end{Bmatrix} \quad (7)$$

where the unknown are the nodal displacements $\{\mathbf{d}\}^1$, the nodal temperatures $\{\mathbf{T}\}^1$ and the nodal pore pressures $\{\mathbf{p}\}^1$ at the current time step, $\{\mathbf{d}\}^0$, $\{\mathbf{T}\}^0$ and $\{\mathbf{p}\}^0$ are the nodal displacements, nodal temperatures, and nodal pore pressures at the previous time step, $\{\mathbf{f}\}$ is the "force" vector, $\{\mathbf{FQ}\}$ and $\{\mathbf{FH}\}$ are heat flux vectors, θ is a time integration constant all the other matrices, [**K**], [**CP**], etc. are assembled from element matrices, which are dependent on thermal, mechanical and hydrological properties of the individual elements and the interpolation functions used. Also

$$c_e = n/K_f - n/K_s + \alpha/K_s$$

$$\beta_e = (1 - \alpha)\beta - (1 - n)\beta_s - n\beta_f.$$

The time integration constant θ varies between 0 and 1. Using a value of $\theta = 0.75$, we observe that after the first few three or four time steps, stability of the solution is generally reliably achieved [22].

3. CODE VERIFICATION

For isothermal cases, analytical solutions for one-dimensional consolidation are given by Terzaghi [9], for two-dimensional plane strain or axisymmetric isothermal consolidation results are given by McNamee and Gibson [23]. References to further studies are given by Selvadurai and Yue [24]. To our knowledge, the only analytical solution under transient conditions and including thermal effects is that given by Booker and Savvidou [25] for the consolidation of an infinite porous medium due to a volumetric heat source. In this chapter we will perform verification of the FRACON code by means of comparison with the above analytical solutions. It is considered that the problems that follow would constitute a useful set of benchmark problems for testing the accuracy of computer codes similar to FRACON.

3.1. One-dimensional isothermal consolidation

Terzaghi [9] provided an analytical solution for the problem of one-dimensional consolidation of a soil column of thickness H, with an impermeable base and loaded at the surface with a constant pressure p_0. The finite element mesh and the boundary conditions for this problem is shown in Fig. 3. The following material parameters are used in the finite element analysis:

$$E = 35 \times 10^9 \text{ Pa}$$

$$\nu = 0.2$$

$$K = 10^{-11} \text{ m/sec.}$$

The load at the surface is assumed to be:

$$p_0 = 30 \times 10^6 \text{ Pa}$$

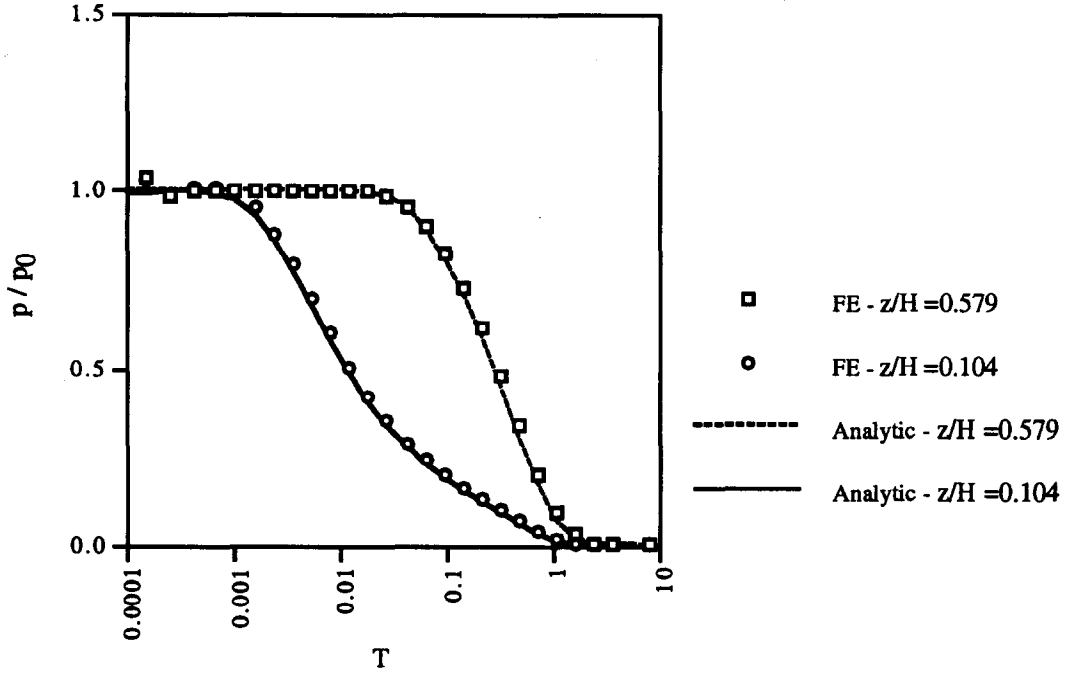

Fig. 4. Pore pressure evolution at different depths.

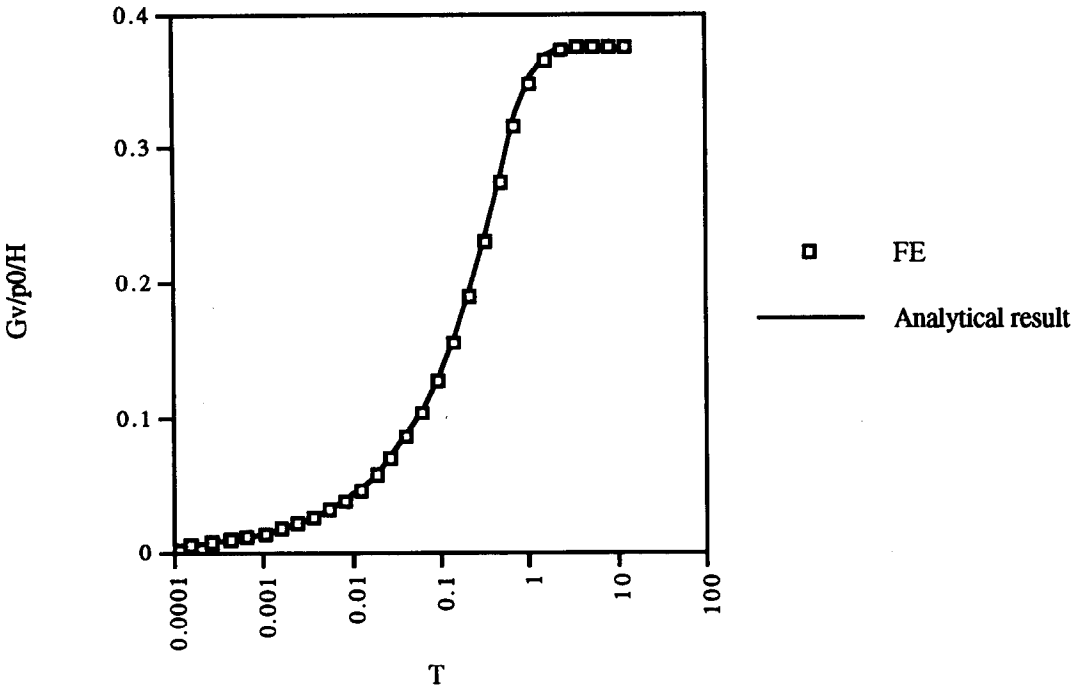

Fig. 5. Vertical settlement of the surface.

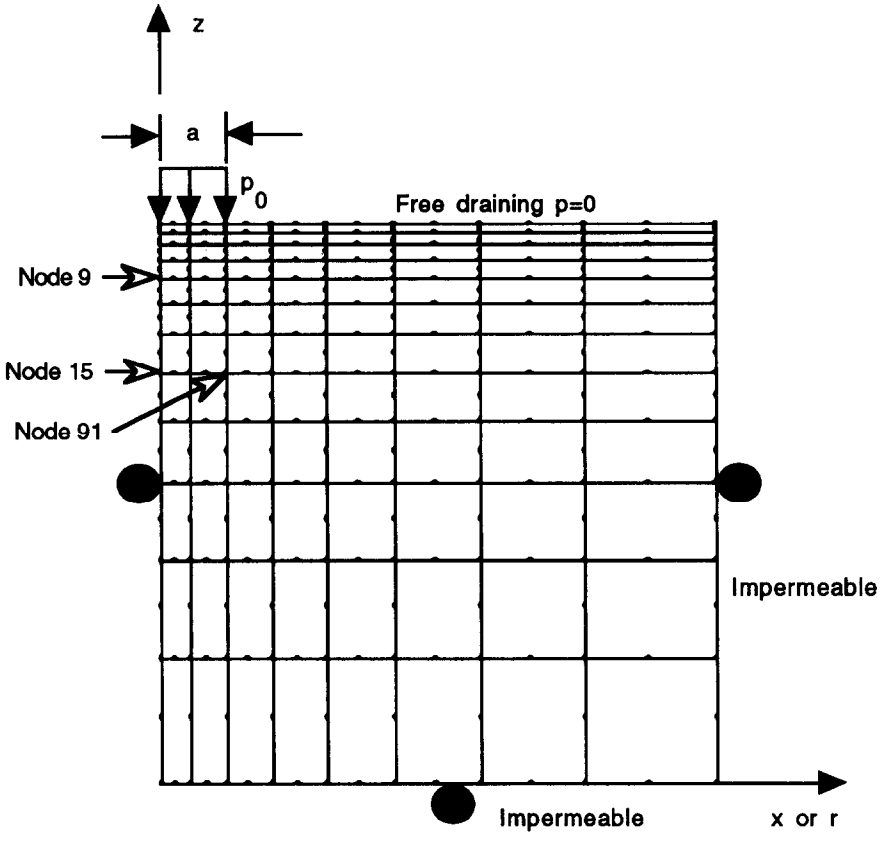

Finite element mesh dimension 50000 mx50000 m
Node 9 : x=0 z=45071
Node 15: x=0 z=37776
Node 91: x=5869 z=36776

Fig. 6. Finite element mesh for consolidation of a half-space under plane strain or axisymmetric conditions.

and the thickness H is:

$$H = 5000 \text{ m}.$$

The normalized pore pressure p/p_0 vs the normalized time T at two different depths z, is shown in Fig. 4, where:

$$T = \frac{c_v t}{H^2} \tag{8}$$

and c_v is the coefficient of consolidation, which is related to the hydraulic conductivity K and the elastic constants by:

$$c_v = \frac{KE(1-v)}{\rho_f g(1-2v)(1+v)} \tag{9}$$

where g is the acceleration of gravity and ρ_f is the density of the pore fluid.

Except for some initial oscillations for the first three of four time steps, Fig. 4 shows that the finite element results agree very accurately with the analytical solution.

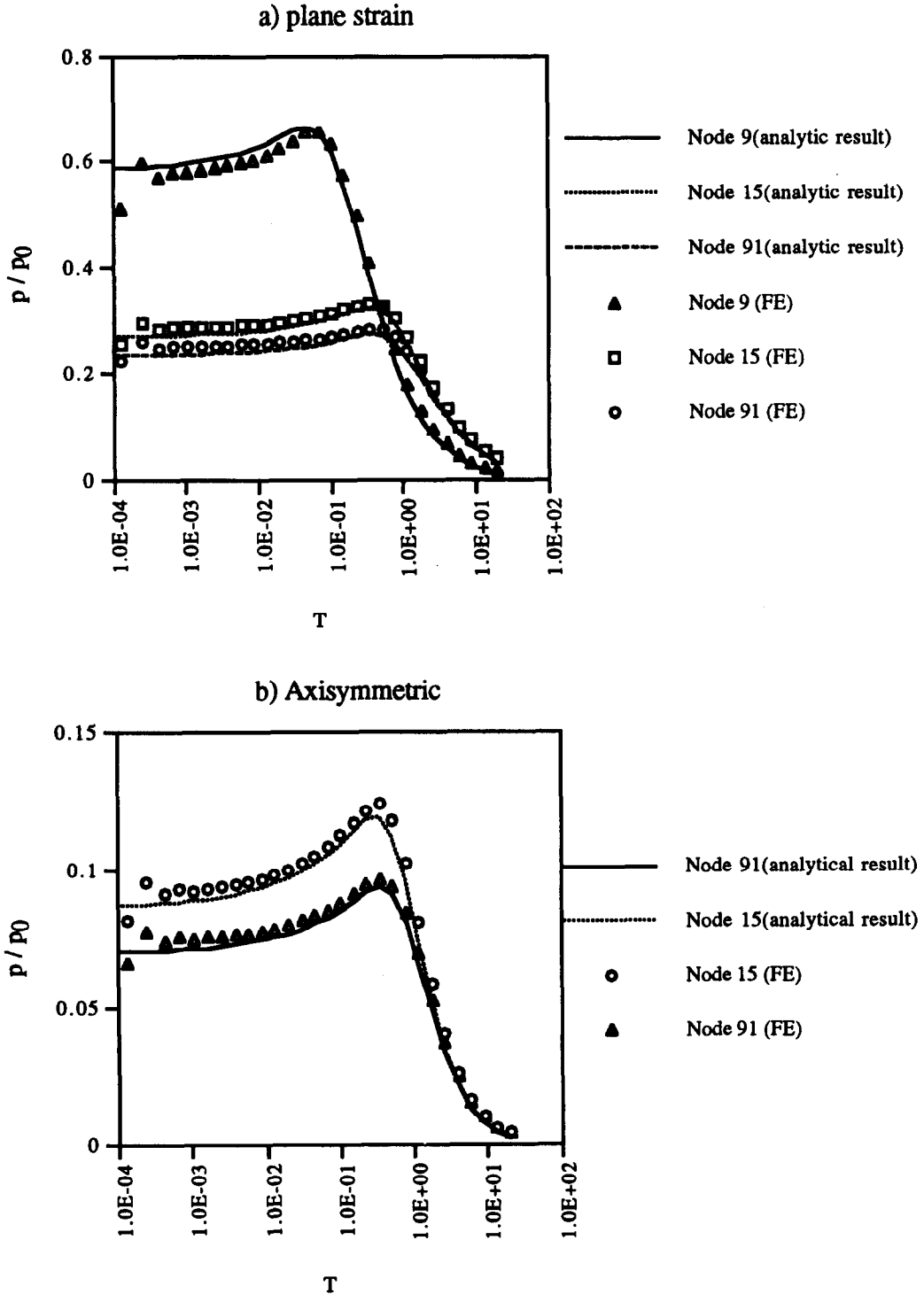

Fig. 7. Plane strain and axisymmetric conditions—pore pressure evolution.

The normalized surface settlement $Gw/p_0/H$ (where G is the shear modulus and w is the absolute settlement) is shown as a function of time in Fig. 5. The agreement between the finite element and the analytical solutions is excellent.

3.2. Isothermal consolidation of a semi-infinite medium under plane strain and axisymmetric conditions

McNamee and Gibson [23] derived analytical solutions for both plans strain and axisymmetric problems of isothermal consolidation of a half-space subject to a load p_0 at the free surface. Under plane strain conditions, the loaded area is a strip of width $2a$, while under axisymmetric conditions, the loaded area is a circular region of diameter $2a$ (see Fig. 6). Expressions for displacements, stresses and pore pressure given by McNamee and Gibson are quite complicated and include integrals which have to be numerically evaluated. Simplifications can be made for the integral expression for the pore pressure in the particular case when the Poisson's ratio is zero i.e.:

$$p(X, Z, T)/p_0 = \int_0^\infty K(X, \xi)\mathrm{e}^{-\xi Z} \times \left\{ \mathrm{erf}(\xi T^{1/2}) + \mathrm{erf}\left(\frac{Z}{2T^{1/2}} - \xi T^{1/2} \right) \right\} \mathrm{d}\xi \quad (10)$$

where:

$X = x/a$, $Z = z/a$ and:

$T = \bar{c}t/a^2$ with $\bar{c} = 2KG/\rho_f/g$ and K is the hydraulic conductivity.

Also,

$$K(X, \xi) = \begin{cases} \dfrac{2}{\pi\xi}\cos(X\xi)\sin\xi & \text{for plane strain} \\ J_0(X\xi)J_1(\xi) & \text{for axisymmetry} \end{cases}$$

erf is the error function, J_0 and J_1 are Bessel functions of order 0 and 1, respectively.

The finite element mesh and the boundary conditions for this problem are shown in Fig. 6. The material parameters used as input data are as follows:

$$a = 5869\ \mathrm{m}$$

$$p_0 = 30 \times 10^6\ \mathrm{Pa}$$

$$E = 35 \times 10^9\ \mathrm{Pa}$$

$$v = 0$$

$$K = 5 \times 10^{-11}\ \mathrm{m/sec.}$$

The numerical and analytical results are compared in Fig. 7(a) for plane strain conditions, and in Fig. 7(b) for axisymmetric conditions. The agreement is quite good, considering the fact that in the finite element analysis, artificial boundaries are introduced at finite distances from the loaded area; consequently, the finite element results are strictly valid only for a finite region. The FRACON code tends to slightly overpredict the values of pore pressure with the boundary conditions shown in Fig. 6. A second analysis, with a zero pore pressure

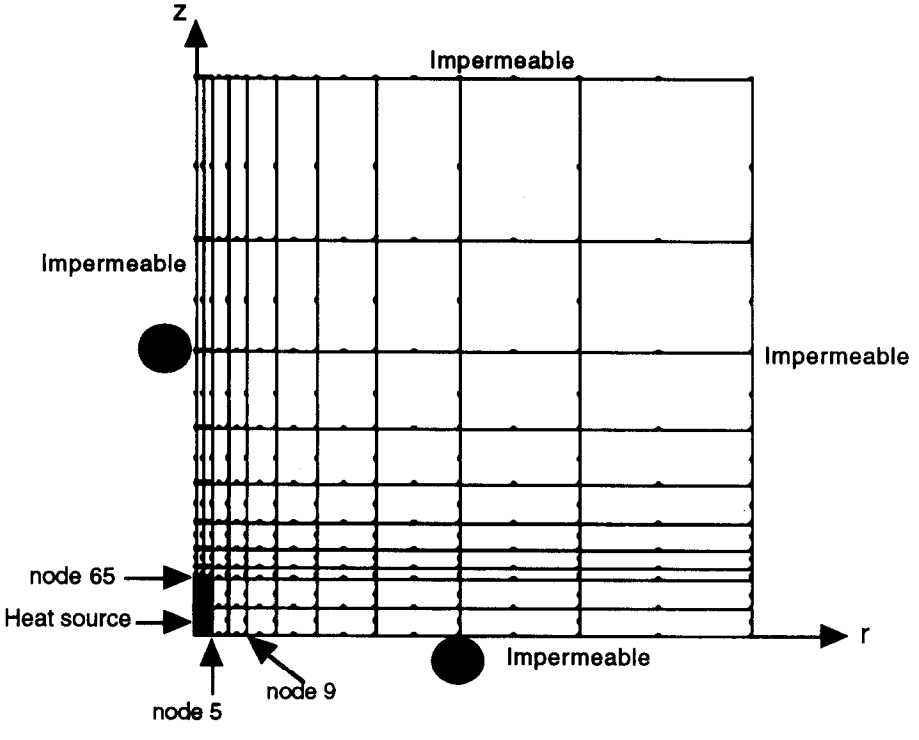

Node 5: x=0.3 z=0
Node 9: x=0.914 z=0
Node 65: x=0 z=1.

Fig. 8. Consolidation of an infinite medium around a cylindrical heat source.

condition specified at the right hand side boundary, was performed with the FRACON code. That resulted in a slight underprediction of the results by the finite element method. For both plane strain and axisymmetric conditions, the Mandel–Cryer effect (i.e. the increase in pore pressure after the immediate increase and before the gradual decrease due to drainage) is manifested at all nodes being considered. The integration of equation (10) is performed numerically with the aid of the mathematical manipulations code MATHEMATICA [26]. For the axisymmetric case, the numerical integration did not converge for node 9. Thus the results for that node are not shown in Fig. 7(b).

3.3. Consolidation of an infinite medium with an embedded cylindrical heat source

An analytical solution was provided by Booker and Savvidou [25] for the consolidation of an infinite homogeneous saturated porous medium, with an embedded volumetric heat source V of constant heat output $q(\mathrm{W/m^3})$. The expressions for the temperature and pore pressure are, respectively:

$$T(x, y, z, t) = \int \frac{q}{4\pi\kappa R} \operatorname{erfc}\left(\frac{R}{2\sqrt{\frac{\kappa}{\rho C}t}}\right) \mathrm{d}V \quad (11)$$

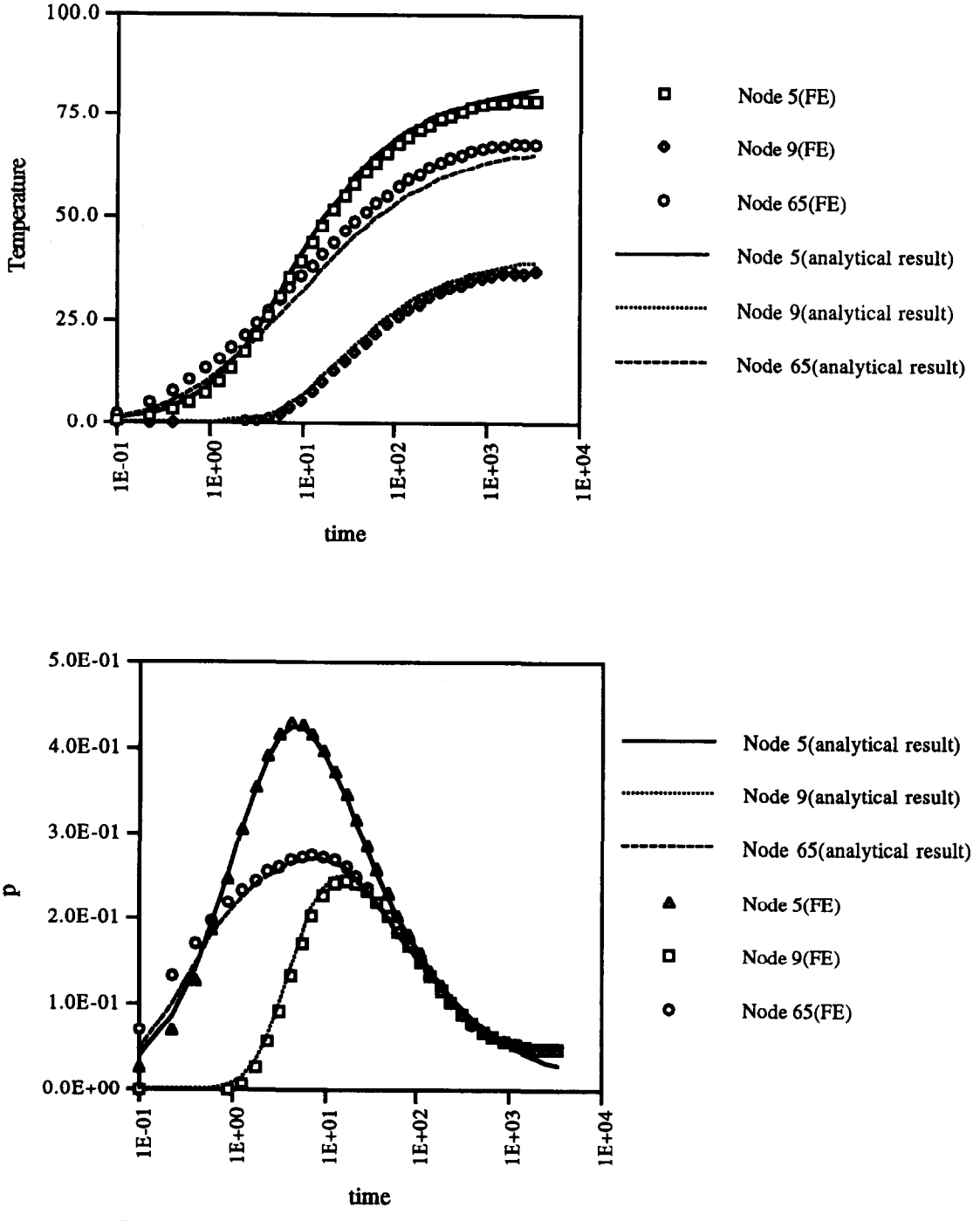

Fig. 9. Cylindrical heat source—temperature and pore pressure evolution at different points.

$$p(x, y, z, t) = \int \frac{X}{1 - \rho C c_v/\kappa} \frac{q}{4\pi\kappa R} \times \left\{ \operatorname{erfc}\left(\frac{R}{2\sqrt{\frac{\kappa}{\rho C} t}} \right) - \operatorname{erfc}\left(\frac{R}{2\sqrt{c_v t}} \right) \right\} dV \quad (12)$$

where:

$$X = [\beta_s(1-n) + n\beta_f](\lambda + 2G) - (\lambda + 2G/3)\beta'$$

$$c_v = K(\lambda + 2G)/\rho_f/g$$

$$R = [(x - x_s)^2 + (y - y_s)^2 + (z - z_s)^2]^{1/2}$$

x_s, y_s, z_s are the coordinates of a point inside the volume V.

We consider here a cylindrical heat source. The same problem has been examined by Lewis and Schrefler [22] using the finite element code PLASCON, using an unspecified but presumably consistent system of units. For comparison purposes, we use here input data similar to those used by Lewis and Schrefler's: radius of cylindrical source: 0.3, height of cylindrical source: 2, $q = 1768.39$, $E = 6000$, $v = 0.4$, $K = 0.4 \times 10^{-5}$, $\kappa = 1.02857$, $\rho C = 40$, $n = 0.5$, $\beta = \beta_s = 0.9 \times 10^{-6}$, $\beta_f = 0.63 \times 10^{-5}$.

The finite element mesh along with the boundary conditions for this problem are shown in Fig. 8. Axisymmetric conditions are specified. The results for temperature and pore pressure at three different nodes are shown in Fig. 9. The FRACON results compare very well with the analytical solutions. It could be seen that at all points, the pore pressure increases due to thermal expansion of the pore fluid, and then gradually dissipates as the medium is allowed to consolidate.

3.4. Consolidation of an infinite medium with an embedded line heat source

We consider here a line source of 1 m length emitting heat at a rate of $q = 40$ W/m. The finite element mesh and the boundary conditions for this problem are shown in Fig. 10. Plane strain conditions are assumed. The line source runs through node 1 shown in Fig. 10. The following properties, typical of an artificial rock used in an experiment performed at Carleton University (cf. Section 4), were used in the analysis: $n = 0.001$, $E = 27$ GPa, $v = 0.24$, $K = 1 \times 10^{-12}$ m/sec, $\kappa = 0.563$ J/m/s/°C, $\rho C = 2 \times 10^6$ J/m^3/°C, $\beta = \beta_s = 0.2 \times 10^{-4}$°C^{-1}, $\beta_f = 0.4 \times 10^{-3}$°C^{-1}.

The temperature and pore pressure at nodes 3 and 9 are shown in Fig. 11. The finite element results are compared with the analytical solutions from Booker and Savvidou [25]. Considering that plane strain assumptions are assumed to simulate a truly three-dimensional problem, the FRACON results are considered to be satisfactory and indicate trends which are consistent with the analytical results.

4. CALIBRATION WITH LABORATORY EXPERIMENT OF AN INTACT SYNTHETIC ROCK

An experiment was performed at Carleton University, Ottawa, Canada to investigate TMH coupling in intact rock. Cementious material was used to simulate hard rock. A cylinder, 50 cm in dia and 47 cm in height was cast with a special mixture of SIKA grout. Thermistors and pore pressure transducers are embedded in the

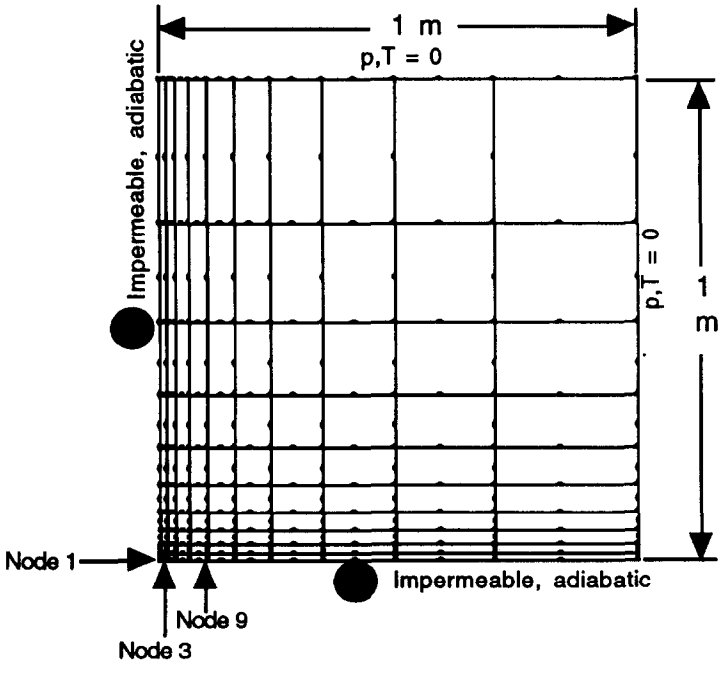

Node 3: x=0.014213 z=0
Node 9: x=0.1 z=0

Fig. 10. Consolidation around a line heat source.

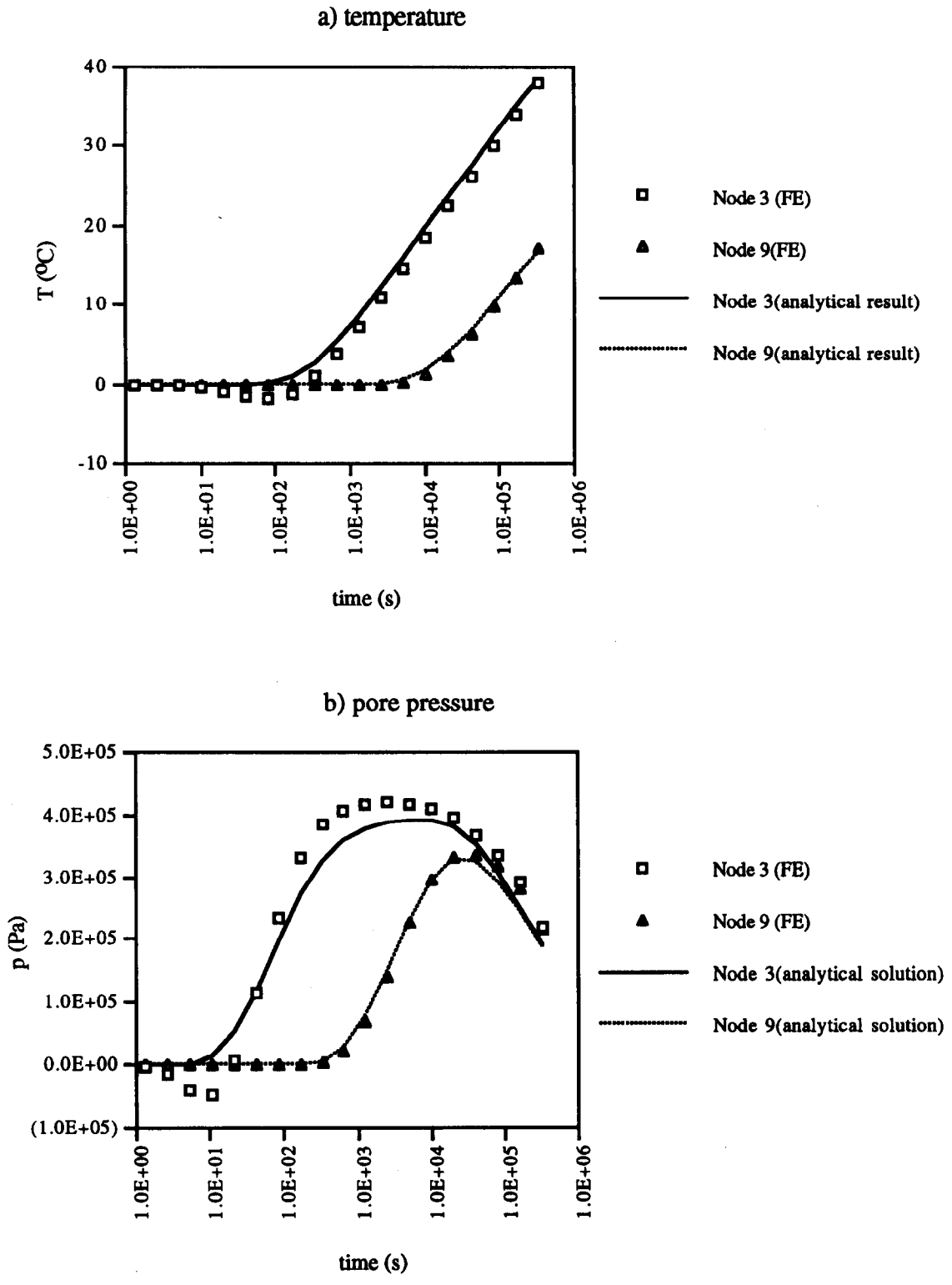

Fig. 11. Line heat source—temperature and pore pressure evolution.

cylinder. The cylinder was vacuum saturated after a 28-day curing period. The cylinder was then immersed in water and a heat source was applied at the surface. Temperatures and pore pressures were continuously recorded by a computerized data acquisition system during the experiment. The properties of the grout material were measured as follows: thermal heat conductivity: $\kappa = 0.563$ J/m/sec/°C, heat capacity: $\rho C = 2 \times 10^6$ J/m^3/°C, Poisson ratio: $\nu = 0.24$, Young's modulus: $E = 26.65$ GPa, coefficient of volumetric thermal expansion of the dry grout: 2×10^{-5}/°C, hydraulic conductivity: 10^{-14}–10^{-12} m/sec.

Further details of the experimental procedures are given in [27]. The laboratory experiment was simulated with the FRACON code, using the above values as input data. The axisymmetric finite element mesh and the relevant boundary conditions are shown in Fig. 12. Since the hydraulic conductivity was very low, undrained conditions were assumed in the analysis. The calculated temperature values agree well with the experimental ones

(Fig. 13). In order to match the calculated pore pressure with the experimental ones, the assumption of slightly imperfect saturation, has to be made. This assumption will result in a modified value of compressibility of the air/water mixture in the pores, as described below.

When the degree of saturation Sr is high ($80\% < Sr < 100\%$) one can neglect capillary and surface tension effects [28]. The porewater/air mixture could then be considered as a homogeneous single phase fluid, albeit with a higher compressibility than pure water. The relation between the compressibility of the equivalent single phase pore fluid and the degree of saturation could be derived as follows.

Consider a vacuum V of the porous medium, with a volume V_v of voids. The void space is occupied partially with water and partially with air. By definition:

$$V_w = V_v Sr \tag{13}$$

$$V_a = V_v(1 - Sr) \tag{14}$$

where V_w and V_a are, respectively, the water and air volumes.

When a pressure dp is applied to the water/air mixture, a volumetric compression in the voids dV_v results, such that:

$$\frac{dV_v}{V_v} = \frac{dV_w}{V_w} Sr + \frac{dV_a}{V_a}(1 - Sr). \tag{15}$$

The compressibility of the air/water mixture is, by definition:

$$C_{aw} = \frac{1}{V_v}\frac{dV_v}{dp} \tag{16}$$

and from (15):

$$C_{aw} = C_w Sr + C_a(1 - Sr) \tag{17}$$

where C_{aw}, C_w, C_a are the compressibilities of, respectively, the air/water mixture, water and air.

Let us assume that the law of ideal gas is valid for air:

$$p_{abs} V_a = mRT \tag{18}$$

where m is the number of moles, R is the universal gas constant, T is the absolute temperature (K) and p_{abs} is the absolute pressure:

$$p_{abs} = p_{atm} + p \tag{19}$$

where p_{atm} is the atmospheric pressure and p is the relative pressure.

Differentiating equation (18) with respect to p, one obtains:

$$C_a = \frac{1}{V_a}\frac{dV_a}{dp} = -\frac{1}{p_{abs}}. \tag{20}$$

Defining compression as positive, and substituting the value of p_{abs} from equation (19) into (20), we obtain:

$$C_a = \frac{1}{p_{atm} + p}. \tag{21}$$

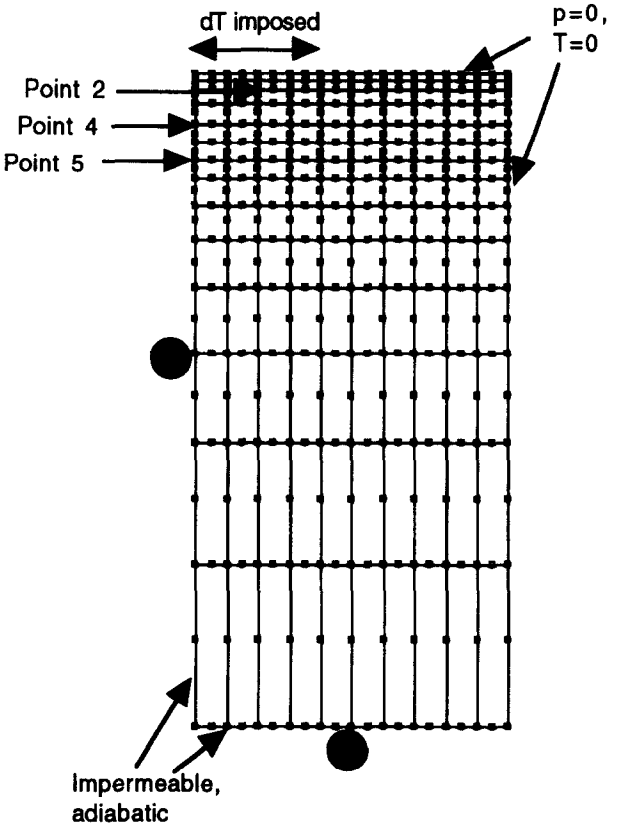

Fig. 12. Heated cylinder—finite element mesh.

Equation (17) then becomes:

$$C_{aw} = C_w Sr + \frac{1 - Sr}{p_{atm} + p}. \tag{22}$$

In the governing equation (3), the bulk modulus of the pore fluid would be:

$$K_f = 1/C_{aw} \tag{23}$$

and would depend on the unknown p, making the equation nonlinear. A direct iteration method was incorporated in the FRACON code to handle this nonlinear behaviour. We assumed that the degree of saturation of the cylindrical block varies from 94 to 99%, with a higher degree of saturation near the outer surface. With these modifications to the degree of saturation, a good match is obtained between the calculated and measured pore pressure values as shown in Fig. 13. Figure 14 shows that the absolute value of the pore pressure is sensitive to Sr, while the time transient is not much affected.

5. SIMULATION OF ROCK MASS RESPONSE TO A NUCLEAR FUEL WASTE REPOSITORY

The FRACON code was used in a preliminary analysis of the performance of a hypothetical repository situated at a depth of 1000 m in a typical pluton of the Canadian Shield. The repository occupies an area of 2000 by 2000 m. It generates heat at an initial rate of 10.4 W/m^2. Due to the decay in radioactivity of the

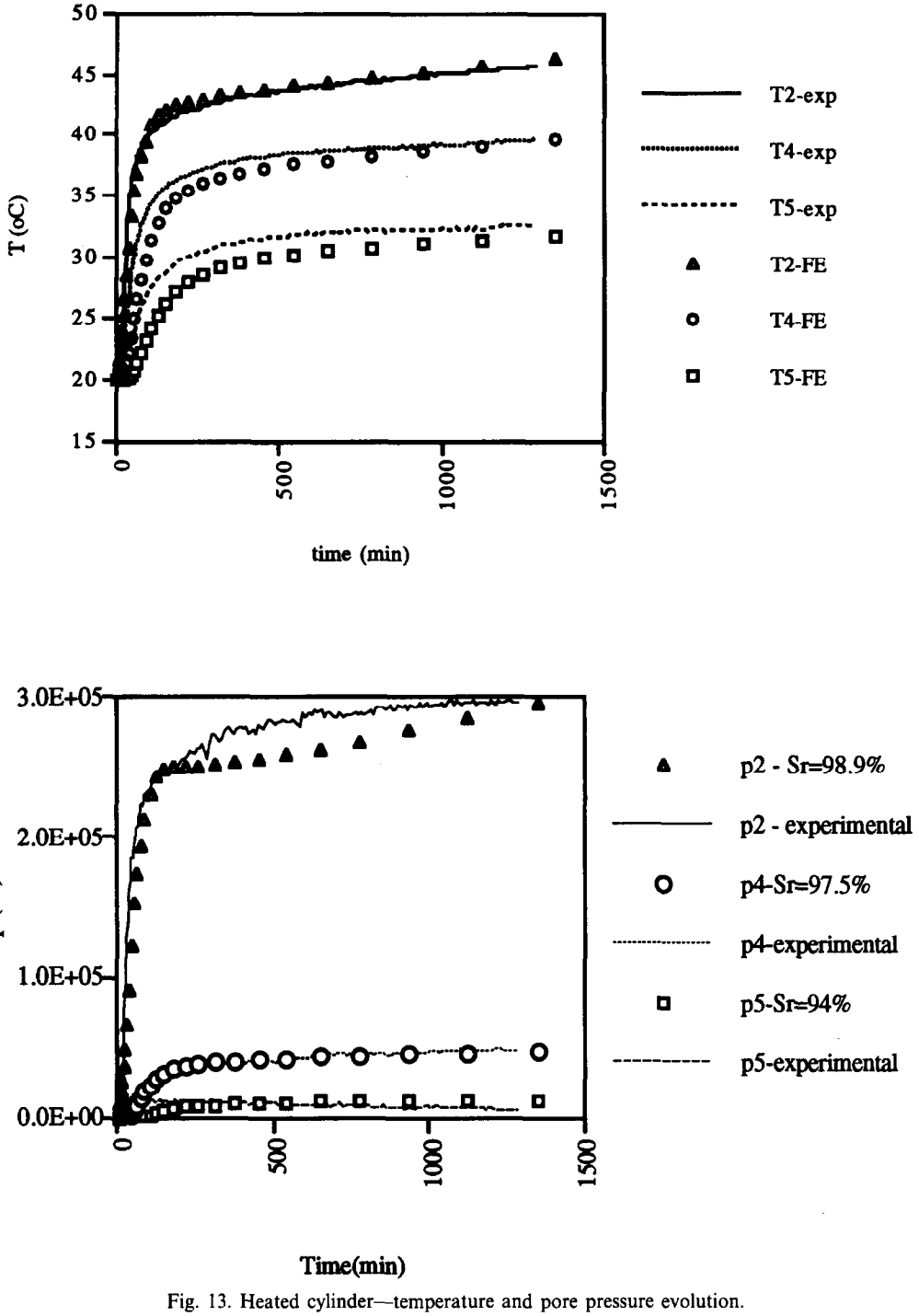

Fig. 13. Heated cylinder—temperature and pore pressure evolution.

wastes, this heat production rate decays to 95% after 1 yr, 80% after 1000 yr and less than 10% after 10,000 yr. It is assumed that two vertical fracture zones, 20 m thick, exists at 100 m from two opposite edges of the repository. Assuming plane strain conditions, the rock mass response was simulated with the FRACON code. The finite element mesh is shown in Fig. 15, along with the boundary conditions. Due to symmetry, only half of the repository was considered. The following thermal-mechanical-hydrological properties of the rock mass are typically applicable to the Canadian Shield [1], and are used in the analysis: Young's modulus and Poisson's ratio: $E = 35$ GPa, $\nu = 0.2$, porosity $n = 0.005$, $k = 3$ W/m/°C, $C = 900$ J/kg°C, density of solids and fluid: $\rho_s = 2700$ kg/m^3, $\rho_f = 1000$ kg/m^3, coefficient of thermal expansion of solid and fluid: $\beta_s = 0.24 \times 10^{-4}$, $\beta_f = 0.4 \times 10^{-3}$, hydraulic conductivity: $K = 1 \times 10^{-11}$ m/sec.

The fracture zone is assumed to have axial and transverse hydraulic conductivities which are three orders of magnitude higher than those applicable to the competent rock mass. Its shear stiffness is assumed to be: $D_{x'y'} = 0.035$ GPa (i.e. three orders of magnitude lower than the Young's modulus of the competent rock mass). Its normal stiffness is assumed to be: $D_{y'y'} = 3.5$ GPa (i.e. one order of magnitude lower than the Young's modulus of the competent rock mass). The thermal conductivity of the fracture zone in both axial and transverse direc-

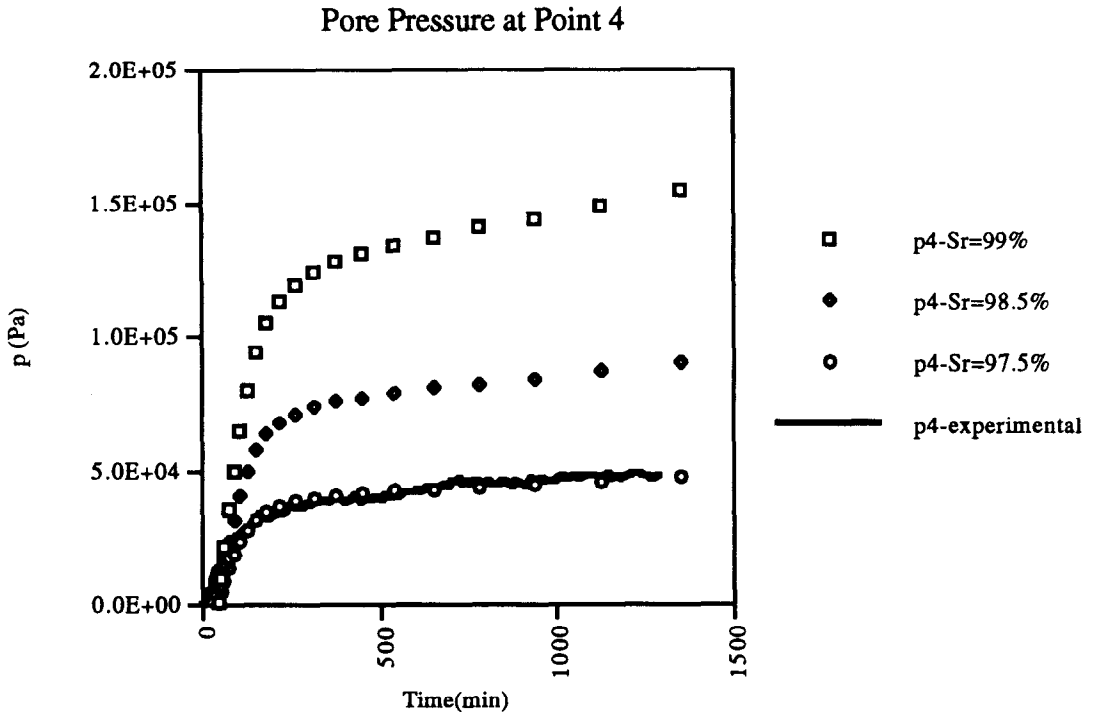

Fig. 14. Heated cylinder—effect of degree of saturation on pore pressure.

tions are assumed to be equal to the one of the rock mass.

The temperature and the pore pressure increases at the center of the repository are shown in Fig. 16. The temperature increase shows two peaks, 50°C at 70 yr and 55°C at 5000 yr; this is consistent with results of others [1]. The pore pressure increase shows a peak of approx. 2.5 MPa at 40 yr. This pore pressure increase is due to the fact that the thermal expansion coefficient of the water is higher than the one of the solid matrix. Due to the low permeability of the medium, drainage is slow and the pore water expansion is impeded, resulting in pore pressure increases in early times. At later times, drainage of water away from the heat source gradually takes place resulting in pore pressure dissipation. Typical contours of pore pressure increases are shown in Fig. 17 (at 40 yr). These gradients can attain values of up to 100% (i.e. several orders of magnitude higher than typical regional gradients in the Canadian Shield which are in the order of 0.1%) resulting in increased groundwater velocities diverging from the repository. Thus, the existing groundwater regimes will be significantly modified by the thermal pulse. One can also see that the fracture zone acts as a drainage feature and would constitute a preferential pathway for groundwater exit to the surface area above the repository. Another implication of these high pore pressures is that effective stresses will be reduced, possibly resulting in a reduction of the strength of both the competent rock mass and the fracture zones.

A typical deformed configuration of the rock mass is shown in Fig. 18. Figure 18 shows that shear movements are induced in the fracture zone, an uplift of the ground surface is induced above the repository and thermal expansion of the rock matrix takes place around the repository. These displacements are only of the order of

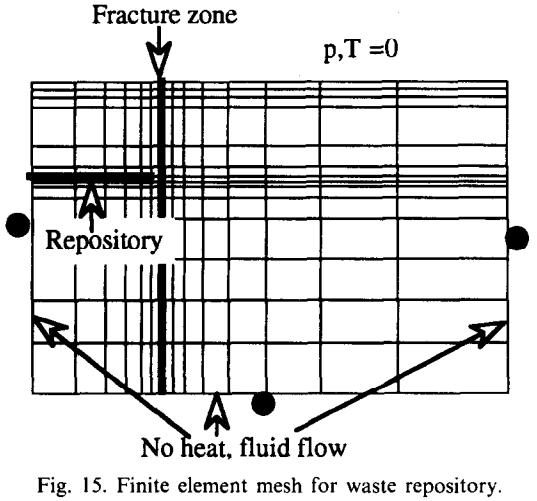

Fig. 15. Finite element mesh for waste repository.

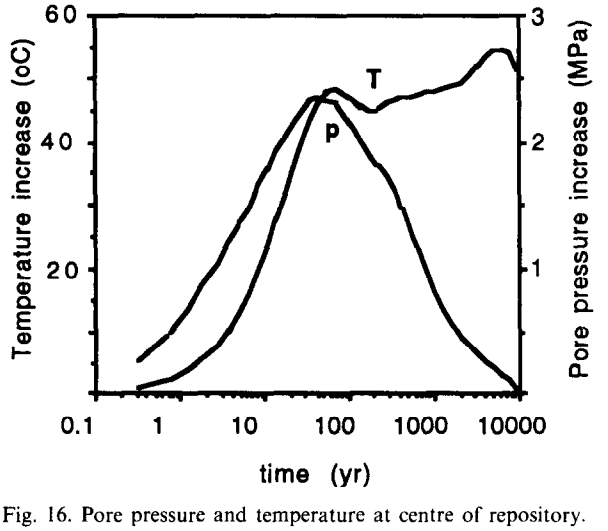

Fig. 16. Pore pressure and temperature at centre of repository.

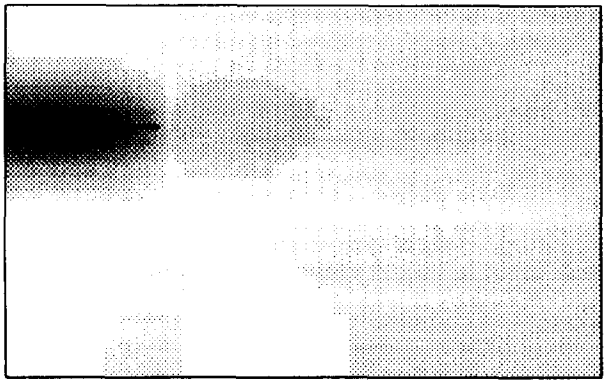

Fig. 17. Typical pore pressure contours at 40 yr after disposal.

centimetres, but they indicate significant disturbances in the stress regime and the structural integrity of the rock mass in the vicinity of the repository. Efforts will be devoted by the authors in the near future to further quantify the above hydrological and mechanical perturbations and their implications on the safety of the repository.

6. CONCLUSION

This paper described the current progress of the AECB's research programme on TMH coupling in sparsely fractured rocks and its implications on Nuclear Fuel waste disposal. As part of this program, a computer code FRACON was developed, tested against analytical solutions, calibrated against a laboratory experiment, and used in the preliminary assessment of the TMH response of a rock mass around a repository. To gain more confidence in the validity of the conceptual model integrated in the FRACON code, laboratory experiments of TMH processes on intact and fractured granitic blocks are in progress at McGill University for calibration/validation purposes. The code is also being currently used to simulate some test cases of DECOVALEX. A detailed analysis to quantify the implications of THM coupling on the safety of a NFW repository will also be performed in the near future.

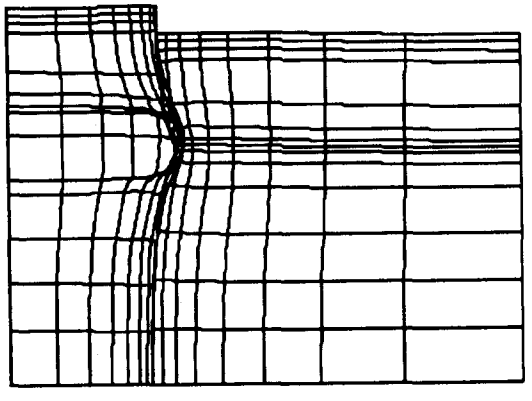

Fig. 18. Deformed mesh.

Acknowledgements—The authors sincerely thank the Atomic Energy Control Board for its financial support, our colleagues at the AECB (D. Bottomley, K. Bragg, P. Flavelle, S. Lei, D. Metcalfe, V. Poliscuk, R. Stenson and J. Wallach) for reviewing this paper, and the laboratory personnel (K. K. Koulourakos, P. Carnaffan and R. Weidelich) at Carleton University for performing the heated block experiment.

Accepted for publication 1 February 1995.

REFERENCES

1. Atomic Energy of Canada Ltd. Used fuel disposal centre—a reference concept. Report TRM-3, AECL Whiteshell, Pinawa, Manitoba, Canada (1992).
2. Nguyen T. S. Canadian concept of nuclear fuel waste disposal—effectiveness of container, buffer and host rock as contaminant barriers. *Proceedings of the 1992 Canadian Geotechnical Conference*, Paper 91 (1992).
3. Cook N. G. W. Coupled processes in geomechanics. In *Coupled Processes Associated with Nuclear Waste Repositories* (Edited by Tsang C. F.), pp. 39–66. Academic Press, New York (1987).
4. Chan T., Reid J. A. K. and Guvanasen V. Numerical modelling of coupled fluid, heat, and solute transport in deformable fractured rock. In *Coupled Processes Associated with Nuclear Waste Repositories* (Edited by Tsang C. F.), pp. 605–626. Academic Press, New York (1987).
5. Norrishad J. and Tsang C. F. Simulation of coupled thermal-hydraulic-mechanical interactions in fluid injection into fractured rocks. In *Coupled Processes Associated with Nuclear Waste Repositories* (Edited by Tsang C. F.), pp. 673–678. Academic Press, New York (1987).
6. Onishi Y., Shibata H. and Kobayashi A. Development of finite element code for the analysis of coupled thermo-hydro-mechanical behaviors of a saturated-unsaturated medium. In *Coupled Processes Associated with Nuclear Waste Repositories* (Edited by Tsang C. F.), pp. 679–698. Academic Press, New York (1987).
7. Witherspoon P. A. The need for field research in coupled processes. In *Coupled Processes Associated with Nuclear Waste Repositories* (Edited by Tsang C. F.), pp. 775–780. Academic Press, New York (1987).
8. SKI (Swedish Nuclear Power Inspectorate). DECOVALEX—Mathematical models of coupled THM processes for nuclear waste repositories. Report of Phase 1. Report SKI TR 93:31, Stockholm, Sweden (1993).
9. Terzaghi K. Die Berechnung der Durchlassigkeitsziffer des Tones aus dem Verlauf der hydrodynamischen Spannungserscheinungen'. *Ak. der Wissenschaften in Wien, Sitzungsberichte mathematisch-naturwissenschaftliche Klasse, Part IIa*, **132**, 125–38, (1923).
10. Biot M. A. General theory in three dimensional consolidation. *J. Appl. Phys.* **12**, 155–164 (1941).
11. Selvadurai A. P. S. and Nguyen T. S. Finite element modelling of consolidation of fractured porous media. *Proceedings of the 1993 Canadian Geotechnical Conference*, pp. 79–88 (1993).
12. Freeze R. A. and Cherry J. A. *Groundwater*. Prentice-Hall (1979).
13. Huyakorn P. S. and Pinder G. F. *Computational Methods in Subsurface Flow*. Academic Press, New York (1983).
14. Rice J. R. and Cleary M. P. Some basic stress diffusion solutions for fluid-saturated elastic porous media with compressible constituents. *Rev. Geophys. Space Phys.* **14**, 227–241 (1976).
15. Zienkiewicz O. C., Hympheson C. and Lewis R. W. A unified approach to soil mechanics problems (including plasticity and viscoplasticity). In *Finite Element in Geomechanics* (Edited by Gudehus G.), pp. 151–178. Wiley, New York (1977).
16. Smith I. M. and Griffiths D. V. *Programming the Finite Element Method*. Wiley, New York (1988).
17. Goodman R. E., Taylor R. L. and Brekke T. L. A model for the mechanics of jointed rock. *J. Soil Mech. Fdn Div. Proc. ASCE* **94**, 637–659 (1968).
18. Zienkiewicz O. C., Best B., Dullage C. and Stagg K. Analysis of non-linear problems in rock mechanics with particular reference to

jointed rock systems. *Proc. 2nd Congr. Int. Soc. Rock Mech.*, Belgrade, Yugoslavia, **3,** 501–509 (1970).
19. Noorishad J., Witherspoon P. A. and Brekke T. L. A method for coupled stress and flow analysis of fractured rock masses. Geotechnical Engineering Publication No. 71–6, Univ. of California, Berkeley (1971).
20. Ghaboussi J., Wilson E. L. and Isenberg J. Finite elements for rock joints and interfaces. *J. Soil Mech. Fdn Div. Proc. ASCE* **99,** 833–848 (1973).
21. Desai C. S. and Nagaraj B. K. Constitutive modelling for interfaces under cyclic loading. In *Mechanics of Material Interfaces* (Edited by Selvadurai A. P. S. and Voyiadjis G. Z.), Vol. II, pp. 97–108. Elsevier, Amsterdam (1986).
22. Lewis R. W. and Schrefler B. A. *The finite element method in the deformation and consolidation of porous media.* Wiley, New York (1987).
23. McNamee J. and Gibson R. E. Plane strain and axially symmetric problems of the consolidation of a semi-infinite clay stratum. *Q. J. Mech. Applied Math.* **XIII,** Pt 2 (1960).
24. Selvadurai A. P. S. and Yue Z. Q. On the indentation of a poroelastic layer. *Int. J. Numerical Analytical Meth. Geomech.* **18,** 161–175 (1994).
25. Booker J. R. and Savvidou C. Consolidation around a point heat source. *Int. J. Numerical Analytical Meth. Geomech.* **9,** 173–184 (1985).
26. Wolfram Research Inc. MATHEMATICA, version 2.2, Champaign, Ill., U.S.A. (1993).
27. Selvadurai A. P. S. Experimental modelling of thermal consolidation around a high level waste repository. AECB INFO doc., Atomic Energy Control Board, Ottawa, Canada. In Press.
28. Vaziri H., Christian H. A. and Pitman T. Generalized form of Terzaghi's consolidation solution. *Proceedings of the 1992 Canadian Geotechnical Conference*, Paper 65 (1992).